This is a “preproof" accepted article for Annals of Glaciology. This version may be subject to change during the production process. 10.1017/aog.2026.10056

Century-scale hindcasting of ice flux using ice-rafted debris as validation: A step toward improved model initialisation

Signe H. LARSEN,[1] Nanna B. KARLSSON,[1] Anne M. SOLGAARD,[1] Synne H. SVENDSEN,[1] Camilla S. ANDRESEN[1]

[1] *Geological Survey of Denmark and Greenland (GEUS), Glaciology and Climate, Copenhagen, DK*

Correspondence: Signe H. Larsen <shl@geus.dk>

ABSTRACT. Assessments of Greenland Ice Sheet dynamics are vital due to the ice sheet's influence on sea level, ocean circulation, and ecosystems. Ice sheet models that simulate these dynamics serve as an important tool for projecting changes under global warming. A key, but understudied, source of uncertainty is the models initial state: small differences can generate large variations in simulated responses to identical climate forcing. Here we address this problem through hindcasting, i.e. creating an initial condition that reproduces past changes on the same timescales as the intended projection. Using a numerical iceflow model, we hindcast Helheim Glacier over the past 127 years and compare the simulations with icebergrafted debris (IRD) records from fjordbed sediment cores to identify the most realistic simulations. Our model configuration reproduced glacier-front retreat and captured ice-flux variability in response to multi-decadal climate forcing fluctuations. Crucially, incorporating IRD records was essential for identifying the most realistic simulations, demonstrating that geological proxies are a valuable and underutilized constraint in ice-sheet modelling.

INTRODUCTION

Modelling the dynamical changes of the Greenland Ice Sheet is important for accurate predictions of future sea-level rise, however, state-of-the-art models disagree on a number of important parameters (Aschwan-

This is an Open Access article, distributed under the terms of the Creative Commons Attribution licence (http://creativecommons.org/licenses/by/4.0), which permits unrestricted re- use, distribution and reproduction, provided the original article is properly cited.

https://doi.org/10.1017/aog.2026.10056 Published online by Cambridge University Press

den and others, 2021; Goelzer and others, 2020; Seroussi and others, 2020), resulting in a large spread in projected estimates. Results from model intercomparison projects like the model initialisation project (InitMIP-Greenland, Goelzer and others, 2018) and the Ice Sheet Model Intercomparison for CMIP6 (ISMIP6, Goelzer and others, 2020) show that differences in a models initial state - such as internal dynamic stability, ice geometry, and subglacial conditions - can, by themselves, produce substantial variation in simulated responses to identical climate forcing. This is deeply problematic for projections of future ice sheet behaviour and impacts ice sheet model fidelity. A possible path toward resolving this issue is to embed hindcasting - the simulation of a historical period on the same timescales as the intended predictions - within the model initialisation workflow. In this approach, models are required to reproduce past changes, which can then be evaluated against observations.

Aschwanden and others (2013) demonstrated how hindcasts validated against observed rates of change in ice thickness, surface speed, and ice discharge reduce the number of acceptable initial states and hence the uncertainty. However, because ice-sheet dynamical adjustments are highly nonlinear and operate on long timescales, a major challenge for hindcasting is that continuous observations of ice-sheet dynamics (e.g. ice flow velocities and thickness changes) span only a few decades, far shorter than the century-scale periods relevant for climate projections. Present-day ice dynamical variability can be reconstructed from satellite observations, with records extending back to the late 1980s. However, even a 40-year satellite record is too short to capture the full range of variability relevant for century-scale projections, given the response time of outlet glaciers (Cuffey and Paterson, 2010). Although historical photographs and mapped trimlines offer valuable constraints on point-in-time conditions (e.g. Bjørk and others, 2012; Khan and others, 2014), they lack temporal continuity. In contrast, geological information, in the form of marine sedimentary archives, can provide proxy time series that extend records of ice dynamical variability beyond the instrumental record.

Here, we explore the potential of using geologically-derived reconstructions of ice flux variability to evaluate model hindcasts. We use the term ice flux to refer to a volume of ice that enters the fjord or ocean as solid ice. Satellite-derived observations of ice fluxes extend back to the late 1980s and are derived from observations of ice velocity and ice thickness. Geological proxies, such as iceberg-rafted debris (IRD) deposited in fjords, provide a continuous proxy record indicating ice flux variability (e.g. Andresen and others, 2012, 2017). IRD is a mixed sedimentary facies of mud, sand and gravel particles, deposited by drifting icebergs as they melt. While not a directly quantified measure of ice flux, IRD variability offers

https://doi.org/10.1017/aog.2026.10056 Published online by Cambridge University Press

important insights into past variability in glacier ice flux and remains largely untapped as a validation tool for ice-sheet models.

In this study, we demonstrate for the first time that IRD can be applied to validate hindcasts. Using the Parallel Ice Sheet Model (PISM, Bueler and Brown, 2009), we generate a small ensemble of 127-year hindcasts of ice flux at Helheim Glacier, each corresponding to a different initial spin-up state. Leveraging information from an IRD record in combination with satellite-derived ice flux and calving-front positions allows us to assess model skill on century timescales and aid us in choosing the ensemble members with the most realistic end states with regards to both geometry and ice discharge, that potentially could form the initial state for century-scale predictions. By applying PISM, built for ice-sheet-scale studies, to a regional setting using simplified climatology, we develop an approach that is transferable to larger domains.

STUDY SITE

Helheim Glacier (Figure 1) is one of Greenlands three largest outlet glaciers in terms of ice flux, contributing roughly 10% of the total Greenland ice-sheet discharge (based on the PROMICE Solid Ice Discharge product Mankoff and others, 2020a,b). It drains a vast catchment of approximately 50,000 km^2 from the southeast sector of the ice sheet into a relatively narrow and uniform branch of Sermilik Fjord that is more than 800 m deep near the terminus (Andresen and others, 2011).

Helheim Glacier has been extensively studied across a range of timescales. At the sub-daily to seasonal scale, GPS and remote sensing observations have captured rapid (hours to days) responses to tidal forcing and meltwater input (Murray and others, 2015; Andersen and others, 2010; Stevens and others, 2016). At the annual scale, variations in terminus position and ice velocity have been linked to seasonal sea-ice cover, fjord circulation patterns, and subglacial discharge (e.g. Ultee and others, 2022; Howat and others, 2005). On multi-decadal time scales, historical photographs and trimline evidence of ice margin position show changes in calving-front position (Bjørk and others, 2012; Khan and others, 2014), while IRD in sediment cores show ice flux changes over the last century (Andresen and others, 2012). Over the past few thousand years, Helheim Glacier likely stabilised during colder periods and increased its discharge during warmer intervals (Andresen and others, 2017), however, compared to many other marine-terminating glaciers, it has remained at a relatively stable calving front position with its present-day extent only a few kilometers inland from its pre-century Little Ice Age (LIA) maximum (Bjørk and others, 2018). We suggest that the reason for this stability is the glaciers large catchment and topographic constraints imposed by the narrow

https://doi.org/10.1017/aog.2026.10056 Published online by Cambridge University Press

and straight Sermilik fjord.

The extensive glaciological studies in combination with the relatively stable ice front position make Helheim Glacier an ideal case for testing century-scale hindcasting methods integrating modern observations with IRD based proxies of ice flux.

DATA AND METHODS

To reconstruct past iceflux variations at Helheim Glacier over the last 127 years, we use the numerical ice-flow model PISM (see section below). Our workflow consists of two stages. First, we generate a quasisteady initial model state that approximates the glaciers geometry around the year 1900. Second, we drive this state forward using reconstructed climate forcings for the 18972024 period and evaluate the simulated flux and model response against available observations. In this section, we first describe the datasets used, and then we detail the PISM configuration and the workflow of the simulations.

Helheim catchment geometry

The Helheim glacier catchment (Figure 1) follows the basin delineation of Mouginot and others (2019), with minor manual adjustments to match surface flow divides derived from the PROMICE ice-velocity winter mosaic (20172018) (Solgaard and Kusk, 2021). Bedrock topography is taken from BedMachine v5 (Morlighem and others, 2022, 2017), and surface topography is the GIMP DEM (Howat and others, 2014) available through the BedMachine dataset (Morlighem and others, 2022). We utilise the AeroDEM digital elevation model derived from aerial photographs in 1981 (Korsgaard and others, 2016) as a reference for glacier geometry during periods when the calving front was more advanced.

Climate data

We use the long-term meteorological record from Tasiilaq (see position in Figure 1), provided by the Danish Meteorological Institute (Cappelen and others, 2020), to extract mean monthly temperature and precipitation from 1897 to the present (Figure 2a). Small gaps in the record are filled manually using data from the same calendar months in previous years. The air temperature record (Figure 2a) shows a pronounced multidecadal signal. After a relatively cold early-1900s, the mean monthly temperature rose at the end of the LIA in the 1920s and continued through the 1960s. This mid-20th-century warm period was followed by a cooler phase spanning the 1970s to the 1990s, before the onset of the present-day warmer

https://doi.org/10.1017/aog.2026.10056 Published online by Cambridge University Press

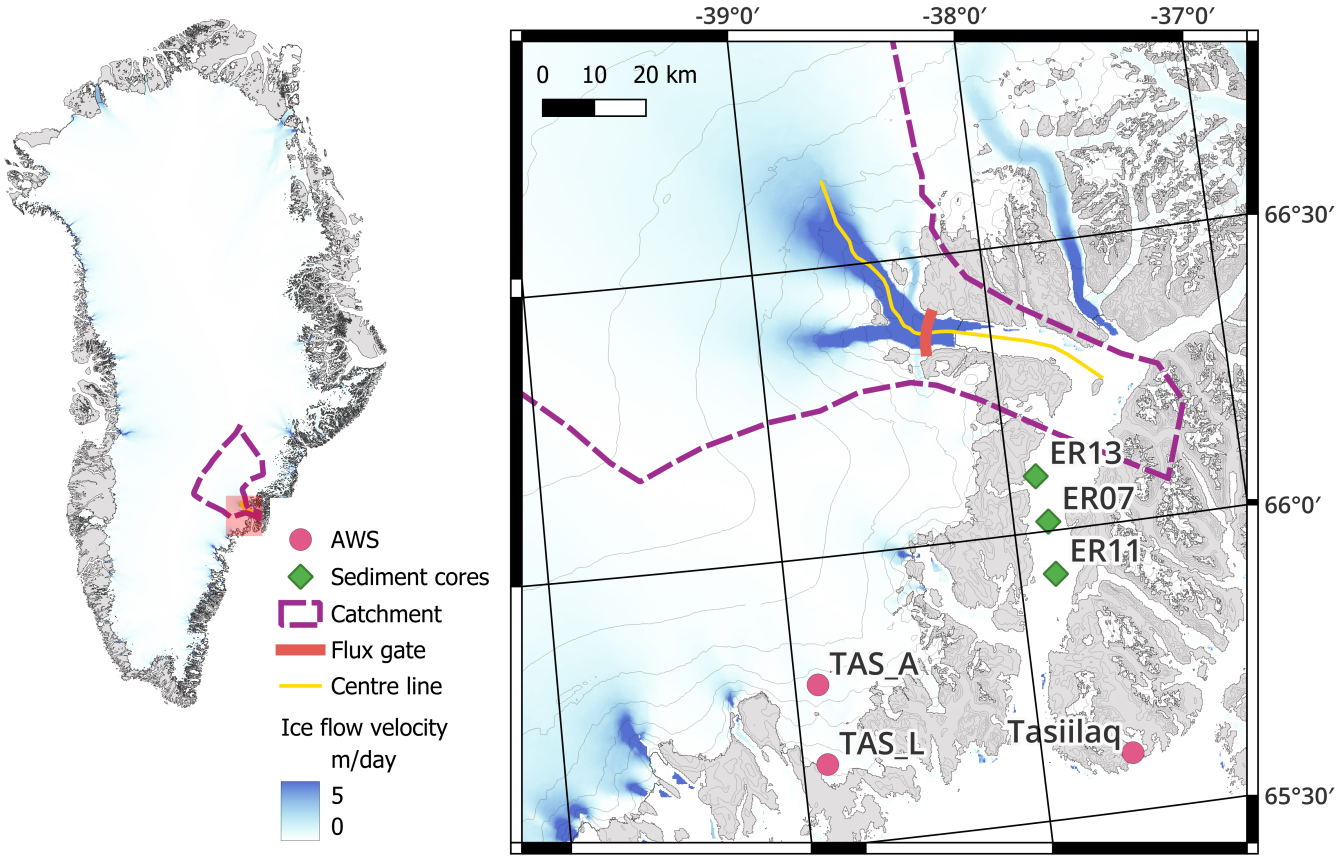


Fig. 1. Left: Greenland with Helheim catchment outlined. Right: The terminus area of Helheim glacier with the ice flux gate from PROMICE Solid Ice Discharge product (Mankoff and others, 2020a,b) in red. Green diamonds mark the positions of the sediment cores from Andresen and others (2012) from which the composite IRD record was generated, red dots mark the locations of the automatic weather stations (AWS) that provide climate data for this study. Background is land and ice masks and elevation contours (200 m contour interval) from BedMachinev5 (Morlighem and others, 2017). Ice flow velocities from the PROMICE Ice Velocity data product are shown in blue colours (Solgaard and Kusk, 2021).

https://doi.org/10.1017/aog.2026.10056 Published online by Cambridge University Press

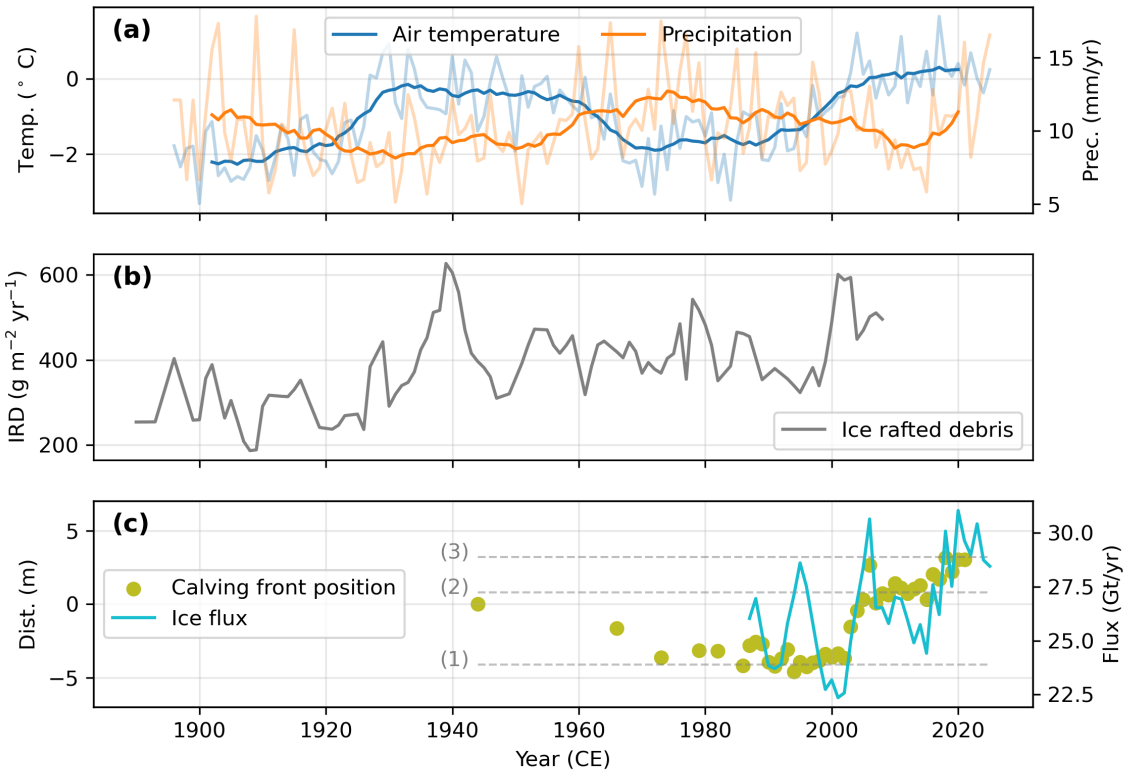


Fig. 2. (a): Observations of air temperature and precipitation from the Danish Meteorological Institute weather station in Tasiilaq from 1897 to 2024 (Cappelen and others, 2020). (b) IRD record (composite of three cores) spanning 1890 to 2008 provided by Andresen and others (2012). (c) Observed calving front positions between 1943 to 2022, from TermPicks database (Goliber and others, 2022; Cheng and others, 2021) shown as distance from the first observation in 1943 (left hand vertical axis) and the ice flux record (right hand axis), between 1986 and 2025, from satellite observations (PROMICE Solid Ice Discharge, Mankoff and others (2020b)). The gray horizontal dashed lines indicate three pinning points where the glacier front is stable for several years.

https://doi.org/10.1017/aog.2026.10056 Published online by Cambridge University Press

phase. This multi-decadal variability is observed in the entire Atlantic region and is sometimes referred to as the Atlantic Multidecadal Variability (e.g. review paper by Zhang and others, 2019). The precipitation record (Figure 2a) reflects this multidecadal variation with lower total precipitation during warm periods.

We construct an artificial cold climate that is needed to relax the model and to construct a reference state for comparison with the model outputs where PISM is forced with the historical climate from Tasiilaq. Relaxing the model here refers to running the simulation under stable boundary conditions until transient dynamical responses to the model initialisation have dissipated to an acceptable degree. The constructed cold climate is simply five successive repetitions of the first 23 years (1897-1920) of our observational period, during which time the climate was relatively cold. The constructed cold climate shows no multi-decadal variability or trend, yet it exhibits natural seasonal and interannual variability, which is important for model output (e.g. Felikson and others, 2022).

To translate temperature information into climate forcing, PISM relies on the positive-degree day model and therefore needs the standard deviation of air temperature over snow/ice. We calculate the standard deviation using data from two PROMICE automatic weather stations (Fausto and others, 2021) located in the vicinity of Helheim Glacier (locations in Figure 1).

Calving front position

Calving-front positions are from the TermPicks database (Goliber and Black, 2021; Cheng and others, 2021), which compiles data from multiple mapping efforts. We use the centreline retreat dataset described in Goliber and others (2022). Data is shown in Figure 2c. At Helheim, the earliest mapped front position in this dataset is from 1943, however, Khan and others (2014) showed the glacier front was likely at the same position as early as 1933. Khan and others (2014) furthermore showed that the glacier front position during the LIA maximum corresponds approximately to the 1985 front position. From the 1940s onward, the front advanced, reaching its maximum observed extent in the 1980s, before undergoing a major retreat in the early 2000s and a further retreat after 2015. Thus, the present glacier front position is the most retreated position in the observational record. Based on the TermPicks database, we infer that the glacier/fjord geometry supports three pinning points, i.e., three locations where the glacier front remained stable for several years. The stable front positions, starting from the most advanced position (dashed gray lines in Figure 2c): (1) 4 km advanced from the first observation (observed in 19852000), (2) around 0 and 0.5 km from the first observation (observed in 1943 and again in 20102015) and (3) around 3 km retreated from

https://doi.org/10.1017/aog.2026.10056 Published online by Cambridge University Press

the first observation (observed in 2021-2024) .

Ice flux

We use the PROMICE Solid Ice Discharge product (Mankoff and others, 2020a,b) which provides ice flux across fixed gates near the marine termini of fast-flowing regions of the Greenland Ice Sheet. The record begins in 1987 with the first ice-velocity measurements from Landsat imagery and is continuously updated to present day. The ice flux records (Figure 2c) show high variability with three distinct peaks: a prominent maximum around 1995, a second peak in the early 2000s and a smaller emerging peak beginning in 2015. The latter two peaks can be associated with substantial calving and glacier front retreat.

Iceberg-rafted debris (IRD)

Iceberg-rafted debris (IRD) consists of sediment (mud and sand) eroded from the glacier bed, entrained within glacial ice, transported by icebergs, and deposited in the fjord during melt. Fine-grained mud is additionally supplied by subglacial meltwater plumes, with deposition decreasing with distance from the glacier front (Andresen and others, 2024). To distinguish between these two sediment sources (icebergs versus meltwater plumes) and isolate iceberg-derived input, sand flux is used as a proxy for iceberg calving activity. Sand grains are too large to be transported by meltwater plumes, so increased sand deposition indicates periods of enhanced iceberg production and, by extension, greater ice discharge from the glacier. However, other processes – such as variations in frozen-fringe and dispersed layer sediment content beneath the ice sheet, iceberg transport time, and oceanographic or climatic conditions that affect iceberg melt in the fjord – may also contribute to IRD variability. In addition, dating of geological records inherently carries uncertainties. Despite these limitations, IRD remains a robust proxy for reconstructing past ice flux as supported by the co-variability between the composite IRD record and historical images of the glacier margin. Increased IRD flux during periods of margin retreat has been documented for Helheim Glacier (Andresen and others, 2012) and other major Greenland outlets, including Sermeq Kujalleq (Wangner and others, 2018), Upernavik Glacier (Vermassen and others, 2019), and Kangerlussuaq Glacier in East Greenland (Vermassen and others, 2020).

Helheim discharges into Sermilik Fjord, where sediment cores have been collected (Andresen and others, 2024). Based on three of these cores (Figure 1, green diamonds), Andresen and others (2012) compiled a composite IRD record that span 1880 to the present. This is the IRD record we use in this study. The

https://doi.org/10.1017/aog.2026.10056 Published online by Cambridge University Press

composite IRD record reports the flux of sand grains (in g m^{-2} y^{-1}) and shows a major increase in IRD flux around the 1930s (Figure 2b). After this peak, the IRD record exhibits sustained high variability and a second rise near the year 2000. Andresen and others (2012) attributed this to a substantial retreat of the calving front, likely marking a transition from its LIA extent to a retreated position in response to the climate warming of the 1920-1940s. The chronologies based on ^{210}Pb and ^{137}Cs carry inherent age uncertainties of approximately 1-3 years at the turn of the 21st century, increasing to 10-20 years in the early 20th century. These uncertainties preclude a direct point-by-point comparison with model output; the comparison is therefore qualitative, focusing on the agreement in general trends and prominent events.

PISM setup

We simulate ice flux using the open-source PISM version 2.1 (Khrulev and others, 2023; Bueler and Brown, 2009). PISM is a numerical model designed to simulate ice sheet dynamics over timescales ranging from centuries to glacial cycles. Studies have demonstrated that the model is able to realistically capture complex flow patterns, including the fast-flowing ice streams characteristic of the Greenland Ice Sheet (Aschwanden and others, 2016). While PISM is widely used for ice-sheet-wide simulations, we configure it here for a regional catchment. Our model setup is briefly described here, focusing on non-default settings and the key input data (a full example of a run command is provided in the Appendix).

General ice physics and basal boundary conditions

We use the hybrid Shallow Ice ApproximationShallow Shelf Approximation (SIASSA) scheme, where the SSA component effectively serves as the sliding law (Bueler and Brown, 2009), enabling realistic representation of both slow-flowing ice and fast-flowing outlet glaciers (Aschwanden and others, 2016). All regional simulations are run on a 1 Œ 1 km grid. Bed topography is held fixed throughout all simulations, as is sea level. Ice sliding follows a non-linear Weertman-type law, modulated by meltwater production at the bed due to frictional and geothermal heat. Ice catchment boundaries are treated as perfect ice divides, prohibiting flux across them. At the ocean boundary, ice that becomes afloat is removed to simulate calving.

https://doi.org/10.1017/aog.2026.10056 Published online by Cambridge University Press

Surface boundary conditions

The climate forcing is introduced at the ice surface. PISM has a built-in atmospheric forcing module that uses temperature and precipitation observations from a weather station and distributes them across the model domain using standard atmospheric lapse rates. We use temperature and precipitation from the DMI weather station at Tasiilaq (Figure 1). Surface mass balance is calculated using a temperature-index melt model described below. Surface melt is computed as proportional to the positive degree days (PDD), with separate degree-day factors for snow and ice. Monthly mean air temperatures from Tasiilaq are converted to PDDs using the semi-empirical formulation of Calov and Greve (2005), which accounts for sub-monthly variability by assuming a normal distribution of daily temperatures around the monthly mean. The mean standard deviation of daily temperature, needed for this method, is derived from the on-ice PROMICE automatic weather stations TAS_A and TAS_L (Figure 1) where we find an average summer (JJA) value of $\sigma = 1.8^{\circ}$C which is applied as a constant throughout the simulation period.

Simulation workflow

We divide the model workflow into three stages:

1. the pre-relaxation stage,

2. the relaxation stage, and

3. the hindcast stage.

The details of each stage are described in the following subsections. Figure 3 visualises the simulation workflow: The left column illustrates the first stage: the pre-relaxation workflow (black and green rectangles). The output from this stage (green rectangle) serves as input to the first relaxation cycle (uppermost blue rectangle). The output at the end of this first relaxation cycle provides initial conditions for the first hindcast (orange rectangle). It is also the starting point for the second relaxation cycle (second blue rectangle), and the output from the second relaxation cycle provides a starting point for the second hindcast (second orange rectangle). This procedure is repeated so that after each relaxation cycle, a hindcast simulation branches off, resulting in seven hindcast simulations, our mini model ensemble.

Importantly, each relaxation cycle also serves as a reference state against which we can compare our hindcast. For example, the first hindcast simulation and the second relaxation cycle have the same initial

https://doi.org/10.1017/aog.2026.10056 Published online by Cambridge University Press

conditions (i.e., the output from the first relaxation cycle). Thus, comparing the first hindcast simulation with the second relaxation cycle reveals the impact of our climate forcings.

The pre-relaxation stage

The aim of the pre-relaxation stage is to create a starting point for our first relaxation cycle. This starting point should be an initial condition with a geometry resembling the geometry of the Helheim catchment around the year 1900 which we assume is the maximum extent during the LIA. Trimline evidence suggests that the glacier front position at the LIA maximum was close to the 1985 position (Khan and others, 2014), which was approximately 7 km further out in the fjord than the present-day position. We therefore use this inferred LIA position to guide the initialisation process. We define a successful initial state as a model state where the calving front is at a position comparable to that of the 1985 calving front. Obtaining a reasonable initial geometry for our relaxation and subsequent hindcast simulations is critical, as multi-decadal changes in ice flux are closely linked to the fjord geometry in the glacier's terminus area (e.g. Nick and others, 2009; Vieli and Nick, 2011; Enderlin and others, 2013).

The initialisation consists of two steps. First, we spin up a Greenland-wide model (black rectangles in Figure 3) to provide a numerically stable starting point for the regional model. Because a Greenland-wide simulation is computationally expensive, we use a grid-sequencing approach in which resolution is progressively refined: the spin-up begins with present-day geometry and runs for 10,000 years at 20 km resolution, followed by 6,000 years at 10 km and 5,000 years at 5 km, under a constant present-day climate. This approach follows the standard spin-up procedure recommended in the PISM documentation (pism.io, last access 21 November 2025). Secondly, from this 5 km Greenland model domain, we extract basal melt rate, till-water-layer thickness, enthalpy, and lithospheric temperature, and interpolate them into a regional domain covering the Helheim glacier catchment at 1 Œ 1 km resolution. The initial ice geometry of this regional model is set to present-day values. The regional model domain is fixed to the dynamic catchment: no ice flux is permitted across lateral boundaries. To minimise artefacts arising from the transition between the Greenland-wide 5 km model and the regional 1 km model, we run PISM for a full cycle of our artificial cold climate with a fixed geometry (green rectangle in Figure 3). This cold climate is shown in Figure 4 (green curve).

https://doi.org/10.1017/aog.2026.10056 Published online by Cambridge University Press

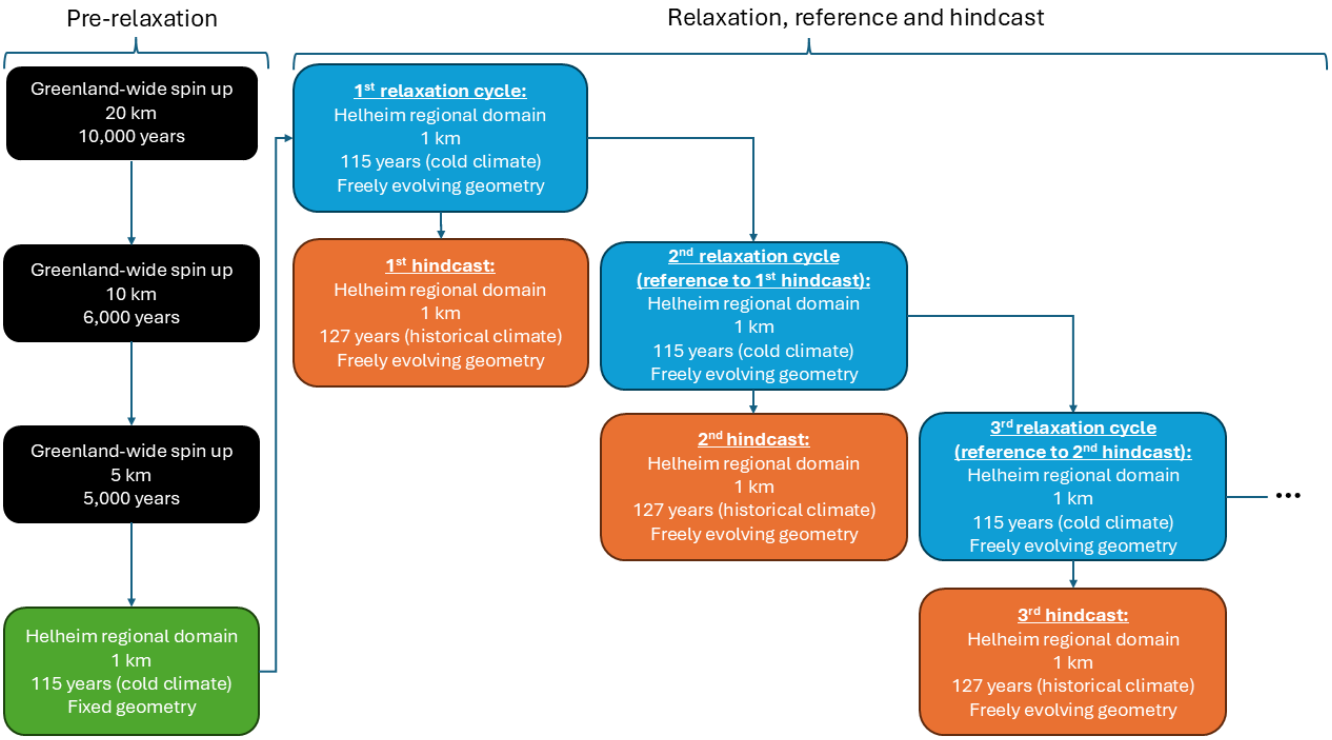


Fig. 3. Workflow of the model run sequence, consisting of pre-relaxation, relaxation, and hindcasting stages. Black denotes model initialisation and green the pre-relaxation step, during which model geometry is held fixed as resolution is downscaled from a 5 km Greenland-wide domain to a 1 km regional domain. The main results are the hindcasts in orange, for each hindcast we can compare against a reference run which corresponds to the relaxation run (blue) from the previous hindcast.

https://doi.org/10.1017/aog.2026.10056 Published online by Cambridge University Press

The relaxation stage

Using the output from the pre-relaxation stage as our first initial conditions, we start the relaxation cycles (blue rectangles in Figure 3). A relaxation cycle is defined by the length of the artificial cold climate (115 years, blue curve in Figure 4) and during the relaxation cycles, the ice geometry may evolve freely at both the iceland and iceocean boundaries. At the end of a relaxation cycle, we assess the final modelled ice geometry to determine whether the ice front remains within the range of observed calving-front positions in the fjord. The calving front at the end of the eighth relaxation cycle has retreated beyond the flux gate, and thus we terminate our simulations at this point and have thereby produced a relaxation run of 920 model years consisting of eight relaxation cycles of 115 years each.

The hindcast stage

We use the final model state at the end of each relaxation cycle as starting points for our hindcasts. Each full 127-year historical hindcast is carried out using observed historical climate forcing (orange curve in Figure 4). This results in seven hindcasts, each branched off from the first seven relaxation cycles. Aside from the climate forcing, and thus the length of the simulation, all aspects of the hindcast are identical to the relaxation cycle. This means that our hindcast ensemble members have been subjected to between 115 and 805 model years of cold climate forcing before the historical climate forcing is introduced. This approach allows us to investigate the effect of the initial state on hindcast results without relying on a steady initial state. Instead of searching for a steady initial state, we can identify the initial state that gives us the most realistic hindcast results. Concurrently, we can assess the impact of the historical climate by comparing the hindcast with the corresponding outputs from the relaxation cycles.

RESULTS

The model simulations yield a mini-ensemble of seven hindcasts, each initiated after an increasingly long relaxation period. We evaluate our results by both looking at the geometry of the initial and end states of the hindcasts as well as the time series of calving front position and simulated ice flux. The initial and final surface elevations from the seven ensemble members along a centre flowline are shown in Figure 5 panel (a) and (b) respectively. Equivalently, Figure 6 show the initial and final mapped ice geometry, panel (a) and (b) respectively, from the seventh hindcast. The calving front positions are extracted along the centre flowline (Figure 1). The ice flux is extracted from the simulated annual maps of ice flux at the grid cells

https://doi.org/10.1017/aog.2026.10056 Published online by Cambridge University Press

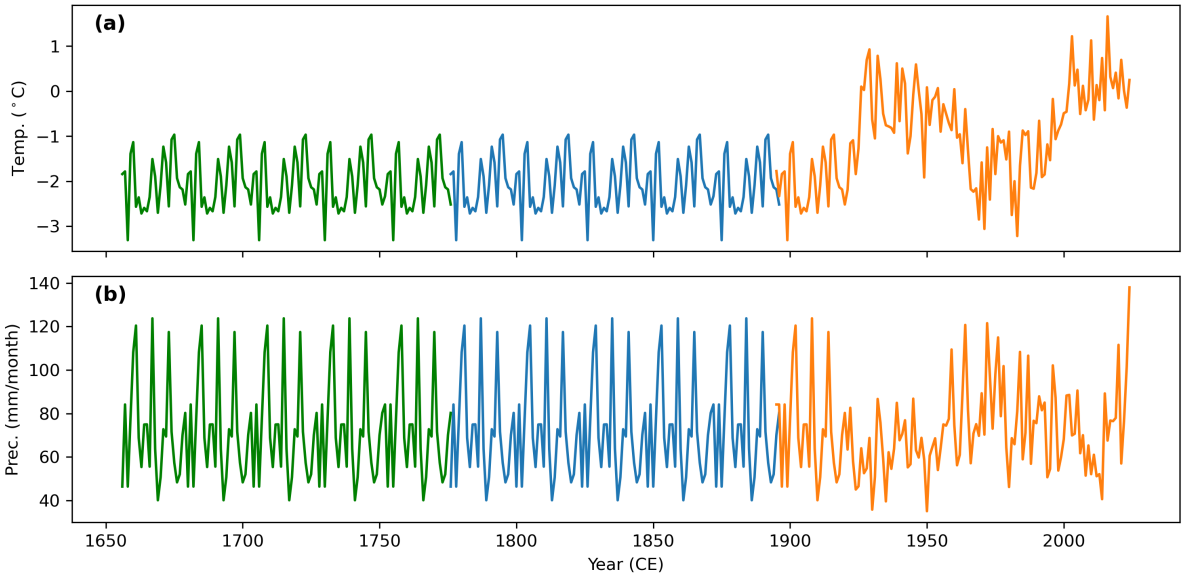


Fig. 4. (a) The temperature forcing applied in the model pre-relaxation (green), relaxation/reference (blue) and historical hindcast (orange). (b) The precipitation forcing applied in the model pre-relaxation (green), relaxation/reference (blue) and historical hindcast (orange).

intersecting the PROMICE solid ice discharge flux gate (Figure 1) and summed to obtain the total gate flux. Since the IRD record serves as an indicator of ice flux variability rather than a direct quantitative measure, and given the inherent age uncertainties of up to 20 years, the comparison between model output and IRD is qualitative and based on visual inspection of the respective curves. Timing offsets of up to 20 years between corresponding features in the two records are considered to be within the uncertainty of the IRD chronology.

Initial states

We define an initial state as the state of the model by the end of a relaxation cycle, which serves as the starting point for our hindcasts. Importantly, we do not aim for initial states that are in steady state. It is unlikely that Helheim Glacier was in a steady state when our historical climate records begin, as the glacier was likely responding to the change in climate following the end of the LIA. Thus, a realistic projection of the future dynamics of Helheim Glacier should reflect this.

Firstly, we note that none of the initial states are in a steady state. This can, for example, be seen in the evolution of the simulated ice surface heights (see Figure 5a), which exhibit a gradual thinning with time, and in the gradual decline of the simulated ice flux throughout the relaxation cycles (Figure 7).

https://doi.org/10.1017/aog.2026.10056 Published online by Cambridge University Press

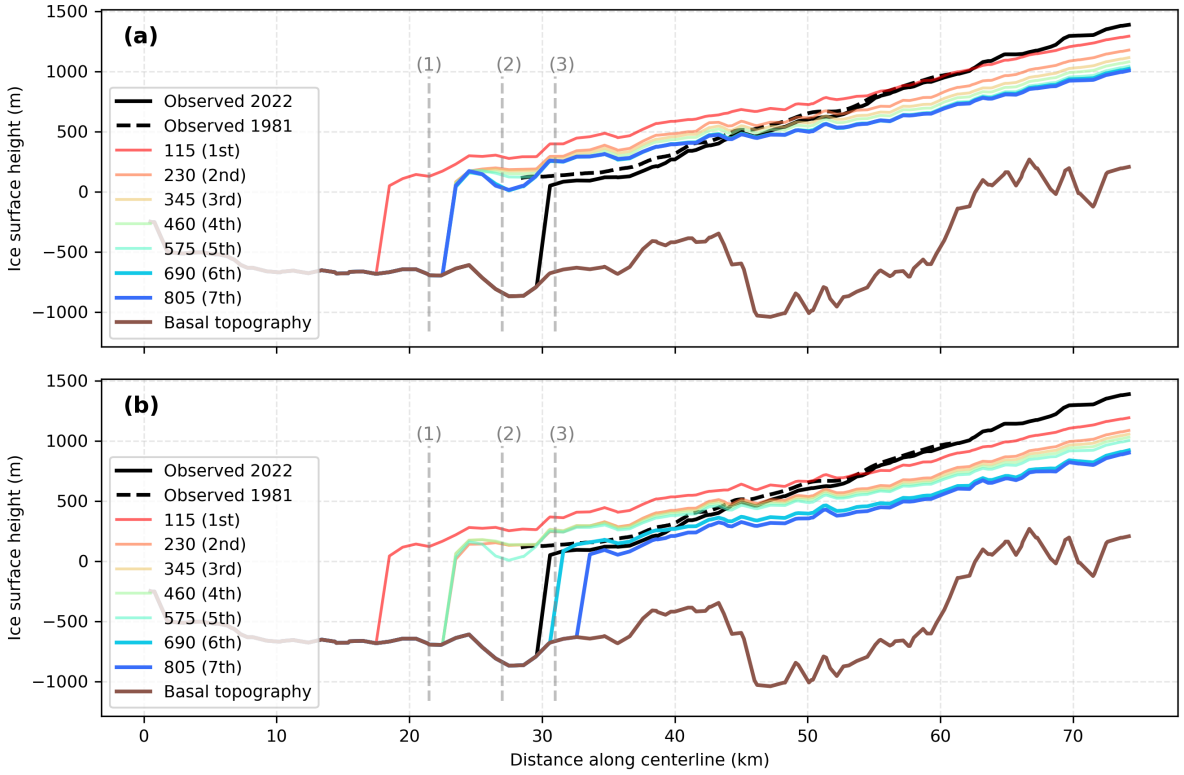


Fig. 5. Surface profiles at the beginning of each hindcast in (a) and at the end of each hindcast in (b) along the centre flowline (Figure 1). Also shown in brown is the basal topography from BedMachine v5 (Morlighem et al., 2022) and the 1981 surface topography in dashed black from AeroDEM (Korsgaard and others, 2016) and in solid black the present day (2009-2016) surface from GIMP DEM (Howat and others, 2014). The grey vertical lines indicate the observed pinning points (Figure 2).

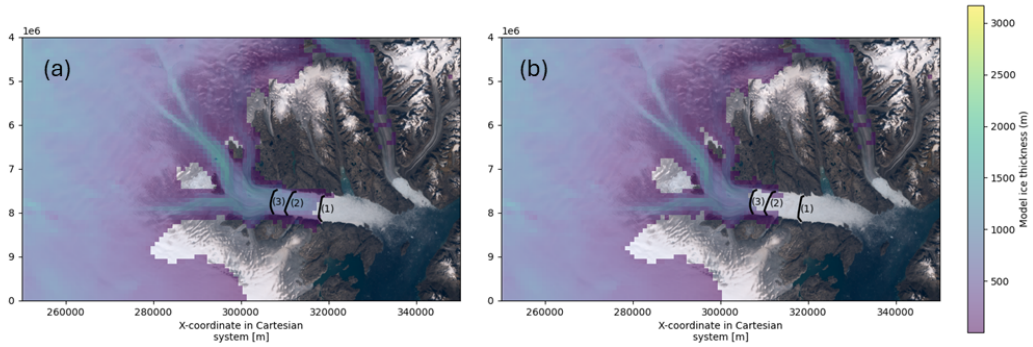


Fig. 6. Geometry of the initial state in panel (a) and the final state in panel (b) of the seventh hindcast. Background map is from Sentinel 2, August 2022. The black lines mark the location of the pinning points of the observed calving front position (Figure 2c.)

https://doi.org/10.1017/aog.2026.10056 Published online by Cambridge University Press

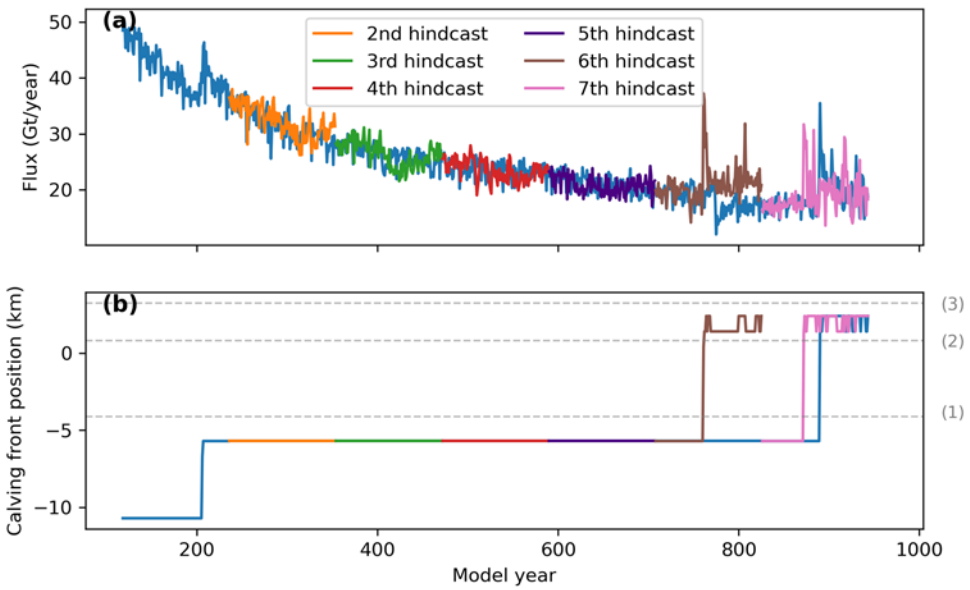


Fig. 7. (a) Simulated ice flux from the model relaxations is shown in blue in consecutive order so that the first relaxation cycle is followed by the second, and the second followed by the third and so on. Overlain are the second to seventh hindcasts in different colours, where each hindcast begins directly after its corresponding relaxation cycle. (b) Simulated calving front positions relative to the observed calving front position in 1943. Blue shows the calving front positions from the relaxation runs in consecutive order, with the calving front positions from the second to seventh hindcasts overlain, as in panel (a). The gray dotted lines mark the three observed pinning points (Figure 2c) for reference.

All initial states excluding the first, have a modelled calving front position close to the likely terminus position at the beginning of 1900 (pinning point (1), see map in Figure 6 and coloured curves in Figure 5a). The elevation profiles for the initial states all show thicker ice near the calving front and thinner ice farther inland compared to observations from 1981 and 2022 (Figure 5a, black curves).

Hindcast simulations

Historical hindcasts were launched from every initial state, and for these hindcasts the model was forced with observed temperature and precipitation for 18972024 (Figure 4). Figure 7 displays the combined simulated ice-flux time series (panel (a)) and calving-front positions (panel (b)) for all simulations that were initiated after two or more relaxation cycles. The relaxation cycles (blue line) and hindcasts (coloured lines) show comparable ice flux from the second to the fifth hindcast. The sixth hindcast (brown line) undergoes major retreat and subsequent ice flux increase that are not seen in the parallel relaxation cycle. Since the retreat did not occur in the parallel (cold) relaxation cycle, the retreat was in fact induced by the

https://doi.org/10.1017/aog.2026.10056 Published online by Cambridge University Press

(warm) historical climate. The seventh hindcast (pink line) also undergoes major retreat, but in this case a similar major retreat also occurs in the parallel relaxation cycle although 19 years later. Thus, in the case of the seventh hindcast, the retreat event appears to be inevitable even with the cold climate forcing, but it occurs earlier due to the warmer historical climate. A map of the model geometry from the seventh hindcast in Figure 6b provides a visualisation of the actual retreat compared to the initial state in Figure 6a.

Comparison to IRD

From the IRD record, we expect a pronounced increase in ice flux around the 1930s, i.e., after 30 years of forcing from the historical climate. The second to fifth hindcast are all initiated with an ice geometry comparable to present day, but they do not show any changes in calving front position or ice flux. Based on this, we consider the sixth and seventh hindcasts to be the most realistic as they retreat at time comparable to when the IRD record indicates changes in ice dynamics.

In Figure 8, we compare the IRD record to the results from the sixth and seventh hindcast simulations, specifically: ice flux and calving front positions. The timing of the retreat is in the 1940s for both hindcast simulations, with the retreat in the seventh hindcast occurring earlier than in the sixth. In both simulations, the increase in simulated ice flux is likely caused by the rapid retreat of the simulated calving front from a stable position close to the maximum observed position (pinning point (2)) to a position close to the present-day position (pinning point (3)). After the retreat, the simulated ice flux remains slightly elevated while the calving front moves back and forth within the distance of one model grid cell. The magnitude and variation of the simulated ice flux resemble those of the observed ice flux (Figure 8, turquoise dots). As also noted above (Figure 7), the retreat in the parallel relaxation cycles happens later than in the simulations forced with the historical climate.

Flux increase at peak ice flux

Comparing hindcast simulations with their parallel reference cycles allows us to quantify the additional ice loss due to the rapid retreat of the calving front. In the sixth hindcast, the ice flux peak spans 1949 to 1955, with a total ice flux of 193 Gt. In the reference run, where no retreat occurs, the total ice flux over the same period was 135 Gt. This means that during 1949 to 1955, the ice discharge was elevated by 43 % compared to a scenario without a retreat. Equivalently, for the seventh hindcast simulation, the peak in

https://doi.org/10.1017/aog.2026.10056 Published online by Cambridge University Press

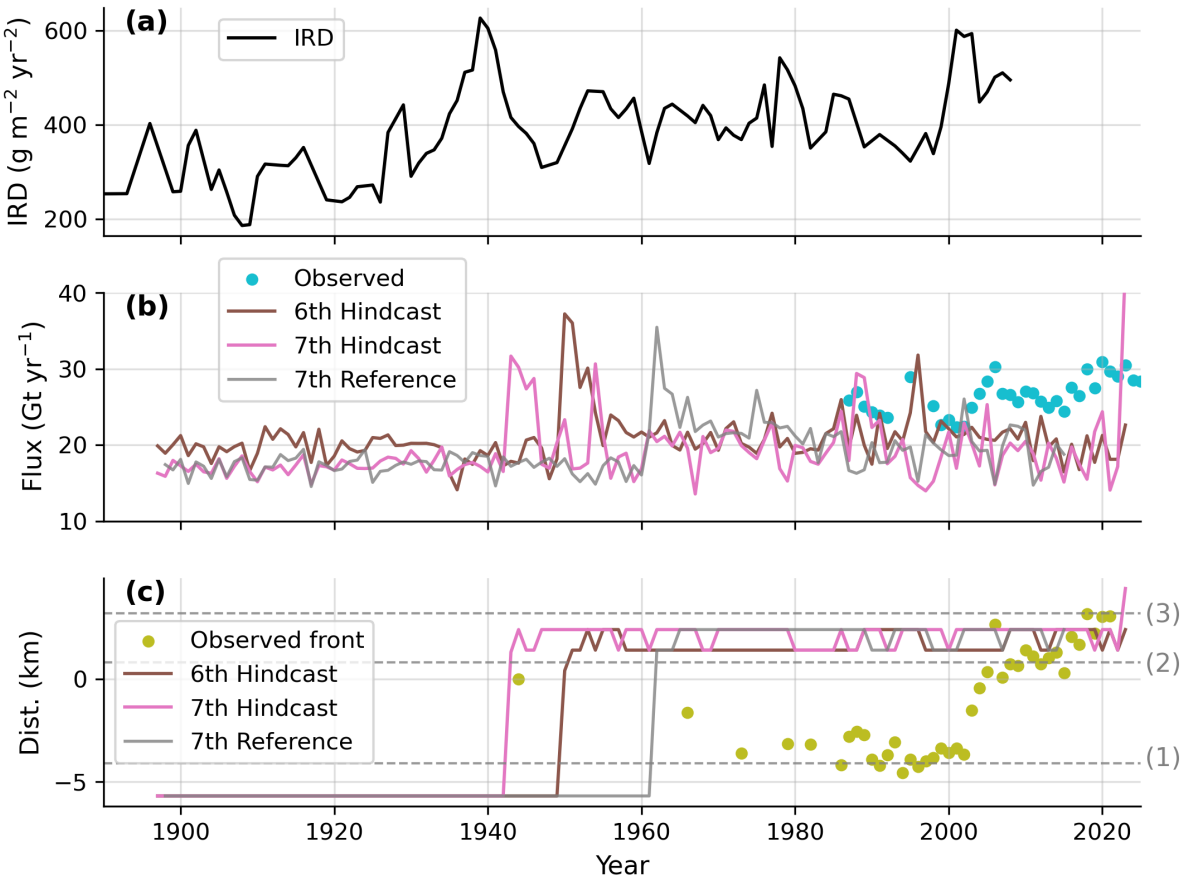


Fig. 8. (a) The observed Ice Rafted Debris (IRD) record, shown for reference to the ice flux variability in panel (b). (b) Simulated ice flux for the selected hindcasts: the sixth hindcast (following six relaxation cycles, i.e. 690 years of relaxation) in brown and the seventh hindcast (following seven relaxation cycles, i.e. 805 years of relaxation) in pink. Blue dots mark the observed ice flux for reference. (c) Simulated calving front distance from the first observed position in 1943 for the selected hindcasts: the sixth hindcast (following six relaxation cycles, i.e. 690 years of relaxation) in brown and the seventh hindcast (following seven relaxation cycles, i.e. 805 years of relaxation) in pink. Green dots mark the observed calving front positions between 1943 and 2022, and gray horizontal lines mark the identified pinning points, shown for reference.

https://doi.org/10.1017/aog.2026.10056 Published online by Cambridge University Press

ice flux begins in 1942 and ends in 1947 and sums up to 147 Gt. The relaxation cycle for the same period sums up to 116 Gt, corresponding to an increase of 26 % in ice flux.

DISCUSSION

The hindcast simulations reproduce the observed magnitude and variability of the ice flux from Helheim Glacier (Figure 8b. Importantly, this is achieved without tuning our ice-flow model to assimilate present-day flow rates or ice thicknesses (Figure 8b), and without starting from a steady state ice geometry. Instead, we choose a non-steady initial state, and this choice is informed by how well the following hindcast simulation reproduces known dynamical changes evident from IRD records and direct observations. While the timing of the modelled retreat does not align precisely with the historical record, this is expected given the uncertainty in the IRD records age model and the simplicity of our experimental design. Without information from the IRD records, multiple end states where ice-sheet geometry matches present-day conditions could have been selected as an initial state, but only two out of the seven they would have produced the required retreat and ice-flux change and would therefore have been a poorer representation of Helheim glacier dynamics. Choosing the best possible initial state enables us to simulate future glacier changes without starting from a steady-state ice-sheet configuration. This is crucial, as the present-day Greenland Ice sheet is not in a steady state but still responding to changes in climate that occurred from the end of the last glacial to the LIA (e.g. Kajanto and others, 2024).

In the most realistic hindcasts (sixth and seventh), the glacier retreat happens rapidly. This rapid retreat is a response to continuous thinning of the ice, which causes the calving front position in the model to retreat from one pinning point to the next pinning point guided by fjord bathymetry (Figure 6). This type of retreat is very similar to the behaviour observed for many marine-terminating glaciers in Greenland (Howat and others, 2005; Joughin and others, 2020; Larsen and others, 2016). The glacier responds to the rapid retreat with a peak in ice flux, which decreases in the years following the retreat. This peak will, for a limited period, cause a higher ice flux, and thus a higher freshwater flux, than if the glacier remained at a stable position. In our simulations, the total ice flux following a retreat was 43 % and 26 % higher for the sixth and seventh hindcast simulation respectively, compared to the same period without a peak in flux. This means that a model simulation that does not accurately capture these rapid retreats will systematically underestimate the total freshwater flux. Thus, our results emphasize that to capture multi-decadal variability in ice flux, it is necessary to correctly capture the geometry of the ice sheet to

https://doi.org/10.1017/aog.2026.10056 Published online by Cambridge University Press

match the timing of retreat events as they directly affect the simulated magnitude of ice flux. Interestingly, even in the cold-climate forcing the glacier front retreats but this retreat happens later compared to the run with the historical forcing. We interpret this as an indication that topography around the outlet of Helheim Glacier, including fjord bathymetry, exerts a strong control on the position of the glacier front.

Comparing the seventh hindcast with the parallel relaxation run (Figure 7) clearly shows that the multi-decadal climate variability has the effect of advancing the time of the retreat event by increasing thinning rates in the mid-century warm period. Thus, emphasising the importance of forcing the model with a realistic variability not only in seasonal climate, as was shown by Felikson and others (e.g. 2022) but also on multi-decadal timescales.

The difference in simulated ice-flux variability between the hindcasts also highlights the well-known problem that the initial state matters for the final results. In our case, the initial state was not in a steady state, just as the ice sheet is not in a steady state when coming out of the LIA. The non-steady state poses a problem of determining whether the initial disequilibrium is a realistic starting point. With this study, we propose a method to solve this problem by hindcasting known changes on timescales comparable to those of relevant future projections, enabled by extending glacier observations back in time using IRD.

Our model setup was unable to simulate the advance of the calving front after the mid-century retreat, which could indicate that the model is too far from a realistic initial state. However, several problems with the boundary conditions may play a larger role than the model setup. Firstly, while the basal topography is crucial for the glacier stability (e.g. Enderlin and others, 2013), it is practically unknown near the terminus of Helheim Glacier and in the fjord in front of the glacier (as seen from the observational data coverage in, for example, Morlighem and others, 2022). The lack of measurements is due to a perpetual cover of icebergs from the calving Helheim glacier. We consider the unknown basal geometry of the historically more advanced glacier to pose the most significant problem for the simulation. Secondly, the spin-up procedure did not account for past climate variability and instead used a relatively warm present-day climate. This may explain why the simulated glacier geometry develops a gentler slope than that observed today. Thirdly, the assumptions regarding basal friction and ice rheology are largely unconstrained. Finally, the iceocean interaction is represented by a constant, low subglacial melt rate despite observations indicating that meltwater-driven plume dynamics and fjord-shelf exchange strongly modulate submarine melt and heat delivery (Muilwijk and others, 2022). Therefore, the lack of modelled glacier re-advance could result from a combination of any or all of these factors.

https://doi.org/10.1017/aog.2026.10056 Published online by Cambridge University Press

While our results are promising and indicate a direction for the future integration of geological records and ice-sheet models, several areas merit further development. These include improving constraints on key parameters such as basal topography and basal friction, addressing model shortcomings and simplifications, and accounting for uncertainties in the geological records and their interpretation.

CONCLUSION

We successfully simulated ice flux and its variability at Helheim Glacier over the past 127 years. By comparing our hindcast simulations with iceberg-rafted debris (IRD) records and historical calvingfront positions, we identified the most realistic initial states for the hindcast. Selecting the optimal initial state allowed us to reproduce a credible retreat event and demonstrates that the IRD geological proxy can improve icesheet model initialisation and validation. Limitations in climate forcing, model assumptions, and glacierfjord geometry preclude simulating the observed advance of the calving front between 1940 and 1970. Consequently, this hindcast cannot serve directly as an initial state for future projections, although the overall methodology remains promising pending further refinements.

Our analysis also reveals that multidecadal variability in climate forcing strongly modulates glacier response, and that models that cannot reproduce rapid retreat events tend to underestimate the total freshwater flux.

By incorporating IRD records directly into the evaluation of our model simulations, we were able to hindcast a century of glacier response to climate change at Helheim Glacier. Producing hindcasts on timescales commensurate with those of the desired projections is key to building confidence in century-scale projections.

CODE AVAILABILITY

The data processing code and PISM run scripts can be found in the GitHub repository:

`https://github.com/GEUS-Glaciology-and-Climate/PISM_Helheim_century`.

ACKNOWLEDGEMENTS

We thank the editor and reviwers for very constructive help for improving This work was supported by the VILLUM Foundation to the project Past and future dynamics of the Greenland Ice Sheet: what is the ocean hiding? (grant no. 10100) and the Programme for Monitoring of the Ice Sheet (PROMICE).

https://doi.org/10.1017/aog.2026.10056 Published online by Cambridge University Press

REFERENCES

Andersen ML, Larsen TB, Nettles M, Elosegui P, As DV, Hamilton GS, Stearns LA, Davis JL, Ahlstrm AP, Juan JD, Ekstrm G, Stenseng L, Khan SA, Forsberg R and Dahl-Jensen D (2010) Spatial and temporal melt variability at Helheim Glacier, East Greenland, and its effect on ice dynamics. *J. Geophys. Res. Earth Surf.*, **115**, 1–18, ISSN 21699011 (doi: 10.1029/2010JF001760)

Andresen CS, Straneo F, Ribergaard MH, a Bjørk A, Andersen TJ, Kuijpers A, Nørgaard-Pedersen N, Kjær KH, Schjøth F, Weckström K and Ahlstrøm AP (2011) Rapid response of Helheim Glacier in Greenland to climate variability over the past century. *Nature Geoscience*, **5**, 37–41, ISSN 1752-0894 (doi: 10.1038/ngeo1349)

Andresen CS, Straneo F, Ribergaard MH, Bjørk AA, Andersen TJ, Kuijpers A, Nørgaard-Pedersen N, Kjær KH, Schjøth F, Weckström K and Ahlstrøm AP (2012) Rapid response of Helheim Glacier in Greenland to climate variability over the past century. *Nature Geoscience*, **5**, 37–41, ISSN 1752-0908 (doi: 10.1038/ngeo1349)

Andresen CS, Kokfelt U, Sicre MA, Knudsen MF, Dyke LM, Klein V, Kaczmar F, Miles MW and Wangner D (2017) Exceptional 20th century glaciological regime of a major SE Greenland outlet glacier. *Scientific Reports*, **7**, 10–17, ISSN 20452322 (doi: 10.1038/s41598-017-13246-x)

Andresen CS, Karlsson NB, Straneo F, Schmidt S, Andersen TJ, Eidam EF, Bjørk AA, Dartiguemalle N, Dyke LM, Vermassen F and Gundel IE (2024) Sediment discharge from Greenlands marine-terminating glaciers is linked with surface melt. *Nature Communications*, **15**, 1332, ISSN 2041-1723 (doi: 10.1038/s41467-024-45694-1)

Aschwanden A, Aðalgeirsdóttir G and Khroulev C (2013) Hindcasting to measure ice sheet model sensitivity to initial states. *The Cryosphere*, 1083–1093 (doi: 10.5194/tc-7-1083-2013)

Aschwanden A, Fahnestock MA and Truffer M (2016) Complex Greenland outlet glacier flow captured. *Nature Communications*, **7**, 10524, ISSN 2041-1723 (doi: 10.1038/ncomms10524)

Aschwanden A, Bartholomaus TC, Brinkerhoff DJ and Truffer M (2021) Brief communication: A roadmap towards credible projections of ice sheet contribution to sea level. *The Cryosphere*, **15**, 5705–5715 (doi: 10.5194/tc-15-5705-2021)

Bjørk AA, Kjær KH, Korsgaard NJ, Khan SA, Kjeldsen KK, Andresen CS, Box JE, Larsen NK and Funder S (2012) An aerial view of 80 years of climate-related glacier fluctuations in southeast Greenland. *Nature Geoscience*, **5**, 427–432, ISSN 1752-0908 (doi: 10.1038/ngeo1481)

Bjørk AA, Aagaard S, Lütt A, Khan SA, Box JE, Kjeldsen KK, Larsen NK, Korsgaard NJ, Cappelen J, Colgan WT, Machguth H, Andresen CS, Peings Y and Kjær KH (2018) Changes in Greenland's peripheral glaciers linked to the North Atlantic Oscillation. *Nature Climate Change*, **8**, 48–52, ISSN 17586798 (doi: 10.1038/s41558-017-0029-1)

https://doi.org/10.1017/aog.2026.10056 Published online by Cambridge University Press

Bueler E and Brown J (2009) Shallow shelf approximation as a "sliding law" in a thermomechanically coupled ice sheet model. *Journal of Geophysical Research: Solid Earth*, **114**, 1–21, ISSN 21699356 (doi: 10.1029/2008JF001179)

Calov R and Greve R (2005) A semi-analytical solution for the positive degree-day model with stochastic temperature variations. *Journal of Glaciology*, **51**, 173–175, ISSN 00221430 (doi: 10.3189/172756505781829601)

Cappelen J, Vinther B, Kern-Hansen C, Laursen EV and Jørgensen PV (2020) Greenland - dmi historical climate data collection 1784-2019. Technical report, Danish Meteorological Institute

Cheng D, Hayes W, Larour E, Mohajerani Y, Wood M, Velicogna I and Rignot E (2021) Calving front machine (calfin): glacial termini dataset and automated deep learning extraction method for greenland, 19722019. *The Cryosphere*, **15**, 1663–1675 (doi: 10.5194/tc-15-1663-2021)

Cuffey KM and Paterson WSB (2010) *The physics of glaciers*. Elsevier, fourth edition, ISBN 9780123694614

Enderlin EM, Howat IM and Vieli A (2013) High sensitivity of tidewater outlet glacier dynamics to shape. *The Cryosphere*, **7**, 1007–1015, ISSN 1994-0424 (doi: 10.5194/tc-7-1007-2013)

Fausto RS, van As D, Mankoff KD, Vandecrux B, Citterio M, Ahlstrøm AP, Andersen SB, Colgan W, Karlsson NB, Kjeldsen KK, Korsgaard NJ, Larsen SH, Nielsen S, Pedersen Ao, Shields CL, Solgaard AM and Box JE (2021) Programme for Monitoring of the Greenland Ice Sheet (PROMICE) automatic weather station data. *Earth System Science Data*, **13**, 3819–3845 (doi: 10.5194/essd-13-3819-2021)

Felikson D, Nowicki S, Nias I, Morlighem M and Seroussi H (2022) Seasonal tidewater glacier terminus oscillations bias multi-decadal projections of ice mass change. *Journal of Geophysical Research: Earth Surface*, **127**, e2021JF006249 (doi: https://doi.org/10.1029/2021JF006249), e2021JF006249 2021JF006249

Goelzer H, Nowicki S, Edwards T, Beckley M, Abe-Ouchi A, Aschwanden A, Calov R, Gagliardini O, Gillet-Chaulet F, Golledge NR, Gregory J, Greve R, Humbert A, Huybrechts P, Kennedy JH, Larour E, Lipscomb WH, clec'h SL, Lee V, Morlighem M, Pattyn F, Payne AJ, Rodehacke C, Rückamp M, Saito F, Schlegel N, Seroussi H, Shepherd A, Sun S, van de Wal R and Ziemen FA (2018) Design and results of the ice sheet model initialisation experiments initMIP-Greenland: an ISMIP6 intercomparison. *The Cryosphere*, **12**, 1433–1460, ISSN 1994-0424 (doi: 10.5194/tc-12-1433-2018)

Goelzer H, Nowicki S, Payne A, Larour E, Seroussi H, Lipscomb WH, Gregory J, Abe-Ouchi A, Shepherd A, Simon E, Agosta C, Alexander P, Aschwanden A, Barthel A, Calov R, Chambers C, Choi Y, Cuzzone J, Dumas C, Edwards T, Felikson D, Fettweis X, Golledge NR, Greve R, Humbert A, Huybrechts P, clec'h SL, Lee V, Leguy G, Little C, Lowry DP, Morlighem M, Nias I, Quiquet A, Rückamp M, Schlegel NJ, Slater DA, Smith RS, Straneo F, Tarasov L, van de Wal R and van den Broeke M (2020) The future sea-level contribution of the Greenland ice sheet: a multi-model ensemble study of ISMIP6. *The Cryosphere*, **14**, 3071–3096 (doi: 10.5194/tc-14-3071-2020)

https://doi.org/10.1017/aog.2026.10056 Published online by Cambridge University Press

Goliber S and Black T (2021) TermPicks: A century of Greenland glacier terminus data for use inmachine learning applications (doi: 10.5281/zenodo.5117931)

Goliber S, Black T, Catania G, Lea JM, Olsen H, Cheng D, Bevan S, Bjørk A, Bunce C, Brough S, Carr JR, Cowton T, Gardner A, Fahrner D, Hill E, Joughin I, Korsgaard NJ, Luckman A, Moon T, Murray T, Sole A, Wood M and Zhang E (2022) TermPicks: a century of greenland glacier terminus data for use in scientific and machine learning applications. *The Cryosphere*, **16**, 3215–3233 (doi: 10.5194/tc-16-3215-2022)

Howat IM, Joughin I, Tulaczyk S and Gogineni S (2005) Rapid retreat and acceleration of Helheim Glacier, east Greenland. *Geophysical Research Letters*, **32** (doi: https://doi.org/10.1029/2005GL024737)

Howat IM, a Negrete and Smith BE (2014) The Greenland Ice Mapping Project (GIMP) land classification and surface elevation data sets. *The Cryosphere*, **8**, 1509–1518, ISSN 1994-0424 (doi: 10.5194/tc-8-1509-2014)

Joughin I, Shean DE, Smith BE and Floricioiu D (2020) A decade of variability on Jakobshavn Isbræ: ocean temperatures pace speed through influence on mélange rigidity. *The Cryosphere*, **14**, 211–227 (doi: 10.5194/tc-14-211-2020)

Kajanto K, Andresen C, Seroussi H, Rieckh T, Briner JP, de Fleurian B, Born A and Nisancioglu K (2024) Holocene warmth explains the Little Ice Age advance of Sermeq Kujalleq. *Quaternary Science Reviews*, **341**, 108840, ISSN 0277-3791 (doi: https://doi.org/10.1016/j.quascirev.2024.108840)

Khan SA, Kjeldsen KK, Kjær KH, Bevan S, Luckman A, Aschwanden A, a a Bjørk, Korsgaard NJ, Box JE, van den Broeke MR, van Dam TM and Fitzner A (2014) Glacier dynamics at Helheim and Kangerdlugssuaq glaciers, southeast Greenland, since the Little Ice Age. *Cryosph.*, **8**, 1497–1507, ISSN 1994-0424 (doi: 10.5194/tc-8-1497-2014)

Khrulev C, Aschwanden A, Bueler E, Brown J, Maxwell D, Albrecht T, Reese R, Mengel M, Martin M, Winkelmann R, Zeitz M, Levermann A, Feldmann J, Garbe J, Haseloff M, Seguinot J, Hinck S, Kleiner T, Fischer E, Damsgaard A, Lingle C, van Pelt W, Ziemen F, Shemonski N, Mankoff K, Kennedy J, Blum K, Habermann M, DellaGiustina D, Hock R, Kreuzer M, Degregori E and Schoell S (2023) Parallel ice sheet model (pism) (doi: 10.5281/zenodo.10202029)

Korsgaard NJ, Nuth C, Khan SA, Kjeldsen KK, Bjørk AA, Schomacker A and Kjær KH (2016) Digital elevation model and orthophotographs of Greenland based on aerial photographs from 19781987. *Scientific Data*, **3**, 160032, ISSN 2052-4463 (doi: 10.1038/sdata.2016.32)

Larsen SH, Khan SA, Ahlstrøm AP, Hvidberg CS, Willis MJ and Andersen SB (2016) Increased mass loss and asynchronous behavior of marine-terminating outlet glaciers at Upernavik Isstrøm, NW Greenland. *Journal of Geophysical Research F: Earth Surface*, **121**, 241–256, ISSN 21699011 (doi: 10.1002/2015JF003507)

https://doi.org/10.1017/aog.2026.10056 Published online by Cambridge University Press

Mankoff KD, Solgaard A, Colgan W, Ahlstrøm AP, Khan SA and Fausto RS (2020a) Greenland Ice Sheet solid ice discharge from 1986 through March 2020. *Earth System Science Data*, **12**, 1367–1383 (doi: 10.5194/essd-12-1367-2020)

Mankoff KD, Solgaard AM and Larsen SH (2020b) Greenland ice sheet solid ice discharge from 1986 through last month

Morlighem M, Williams CN, Rignot E, An L, Arndt JE, Bamber JL, Catania G, Chauché N, Dowdeswell JA, Dorschel B, Fenty I, Hogan K, Howat I, Hubbard A, Jakobsson M, Jordan TM, Kjeldsen KK, Millan R, Mayer L, Mouginot J, Noël BPY, O'Cofaigh C, Palmer S, Rysgaard S, Seroussi H, Siegert MJ, Slabon P, Straneo F, van den Broeke MR, Weinrebe W, Wood M and Zinglersen KB (2017) Bedmachine v3: Complete bed topography and ocean bathymetry mapping of greenland from multibeam echo sounding combined with mass conservation. *Geophysical Research Letters*, **44**(21), 11,051–11,061 (doi: https://doi.org/10.1002/2017GL074954)

Morlighem M, and others (2022) IceBridge BedMachine Greenland (IDBMG4, Version 5) [data set]

Mouginot J, Rignot E, Bjørk AA, van den Broeke M, Millan R, Morlighem M, Noël B, Scheuchl B and Wood M (2019) Forty-six years of Greenland Ice Sheet mass balance from 1972 to 2018. *Proceedings of the National Academy of Sciences of the United States of America*, **116**, 9239–9244, ISSN 10916490 (doi: 10.1073/pnas.1904242116)

Muilwijk M, Straneo F, Slater DA, Smedsrud LH, Holte J, Wood M, Andresen CS and Harden B (2022) Export of ice sheet meltwater from Upernavik Fjord, West Greenland. *Journal of Physical Oceanography*, **52**, 363 – 382 (doi: 10.1175/JPO-D-21-0084.1)

Murray T, Selmes N, James TD, Edwards S, Martin I, O'Farrell T, Aspey R, Rutt I, Nettles M and Baugé T (2015) Dynamics of glacier calving at the ungrounded margin of Helheim Glacier, southeast Greenland. *Journal of Geophysical Research: Earth Surface*, **120**, 964–982 (doi: https://doi.org/10.1002/2015JF003531)

Nick FM, Vieli A, Howat IM and Joughin IR (2009) Large-scale changes in greenland outlet glacier dynamics triggered at the terminus. *Nature Geoscience*, **2**, 110–114, ISSN 1752-0894 (doi: 10.1038/ngeo394)

Seroussi H, Nowicki S, Payne AJ, Goelzer H, Lipscomb WH, Abe-Ouchi A, Agosta C, Albrecht T, Asay-Davis X, Barthel A, Calov R, Cullather R, Dumas C, Galton-Fenzi BK, Gladstone R, Golledge NR, Gregory JM, Greve R, Hattermann T, Hoffman MJ, Humbert A, Huybrechts P, Jourdain NC, Kleiner T, Larour E, Leguy GR, Lowry DP, Little CM, Morlighem M, Pattyn F, Pelle T, Price SF, Quiquet A, Reese R, Schlegel NJ, Shepherd A, Simon E, Smith RS, Straneo F, Sun S, Trusel LD, Breedam JV, van de Wal RSW, Winkelmann R, Zhao C, Zhang T and Zwinger T (2020) ISMIP6 Antarctica: a multi-model ensemble of the antarctic ice sheet evolution over the 21st century. *The Cryosphere*, **14**, 3033–3070 (doi: 10.5194/tc-14-3033-2020)

Solgaard AM and Kusk A (2021) Winter ice velocity mosaics for the greenland ice sheet from sentinel-1 edition 1

https://doi.org/10.1017/aog.2026.10056 Published online by Cambridge University Press

Stevens LA, Behn MD, Das SB, Joughin IR, Noël B, van den Broeke MR and Herring T (2016) Greenland ice sheet fl ow response to runoff variability. *Geophysical Research Letters*, 1–9 (doi: 10.1002/2016GL070414.Received)

Ultee L, Felikson D, Minchew B, Stearns LA and Riel B (2022) Helheim Glacier ice velocity variability responds to runoff and terminus position change at different timescales. *Nature Communications*, **13**, ISSN 20411723 (doi: 10.1038/s41467-022-33292-y)

Vermassen F, Wangner DJ, Dyke LM, Schmidt S, Cordua AE, Kjær KH, Haubner K and Andresen CS (2019) Evaluating ice-rafted debris as a proxy for glacier calving in Upernavik Isfjord, NW Greenland. *Journal of Quaternary Science*, **34**, 258–267 (doi: https://doi.org/10.1002/jqs.3095)

Vermassen F, Bjørk AA, Sicre MA, Jaeger JM, Wangner DJ, Kjeldsen KK, Siggaard-Andersen ML, Klein V, Mouginot J, Kjær KH and Andresen CS (2020) A major collapse of Kangerlussuaq Glacier's ice tongue between 1932 and 1933 in east Greenland. *Geophysical Research Letters*, **47**, e2019GL085954 (doi: https://doi.org/10.1029/2019GL085954), e2019GL085954 2019GL085954

Vieli A and Nick FM (2011) Understanding and modelling rapid dynamic changes of tidewater outlet glaciers: Issues and implications. *Surveys in Geophysics*, **32**, 437–458, ISSN 0169-3298 (doi: 10.1007/s10712-011-9132-4)

Wangner DJ, Jennings AE, Vermassen F, Dyke LM, Hogan KA, Schmidt S, Kjær KH, Knudsen MF and Andresen CS (2018) A 2000-year record of ocean influence on Jakobshavn Isbræ calving activity, based on marine sediment cores. *The Holocene*, **28**, 1731–1744 (doi: 10.1177/0959683618788701)

Zhang R, Sutton R, Danabasoglu G, Kwon YO, Marsh R, Yeager SG, Amrhein DE and Little CM (2019) A review of the role of the atlantic meridional overturning circulation in Atlantic multidecadal variability and associated climate impacts. *Reviews of Geophysics*, **57**, 316–375 (doi: https://doi.org/10.1029/2019RG000644)

APPENDIX

An example of PISM run script, in this case the set-up for the first relaxation cycle, all scripts and more details are available in the GitHub repository:

`https://github.com/GEUS-Glaciology-and-Climate/PISM_Helheim_century`

```
#!/bin/bash
E=3
dT=-6.5
dPdz=-0.095
```

https://doi.org/10.1017/aog.2026.10056 Published online by Cambridge University Press

```
temp_sd=1.8
EXDT=1
EXVARS='thk,velsurf_mag,surface_melt_rate,surface_runoff_rate'
TSTIME=monthly
BOOT=no_mass_E${E}_v4.0.nc
OUTFILENAME=relax_1st_cycle_calvingNG_false_calvingM_false_E3_v4.2

# check if env var PISM_DO was set (i.e. PISM_DO=echo for a 'dry' run)
if [ -n "${PISM_DO:+1}" ] ; then
  echo "$SCRIPTNAME         PISM_DO = $PISM_DO  (already set)"
else
  PISM_DO=""
fi
PROJ_LIB=/usr/share/proj
PISM_ONESTATION=pism_one_station_tas_cold_noleap-with-bounds.nc
PISM_DATANAME=force_to_thickness_v2_ftt.nc

regridcommand="-regrid_file $BCFILE -regrid_vars basal_melt_rate_grounded,tillwat,enthalpy,litho_tem

CLIMATE="-atmosphere one_station,elevation_change \
     -atmosphere.one_station.file $PISM_ONESTATION \
     -atmosphere.elevation_change.file $BOOT \
     -atmosphere.elevation_change.temperature_lapse_rate $dT \
     -atmosphere.elevation_change.precip_adjustment shift \
     -atmosphere.elevation_change.precipitation.lapse_rate $dPdz \
     -surface pdd,forcing \
     -force_to_thickness_file $PISM_DATANAME \
     -surface.pdd.std_dev.value ${temp_sd} \
     -sea_level constant "
```

https://doi.org/10.1017/aog.2026.10056 Published online by Cambridge University Press

```
PHYS="-pik \
      -sia_e ${E} \
      -stress_balance ssa+sia \
      -topg_to_phi 15.0,40.0,-300.0,700.0 \
      -till_effective_fraction_overburden 0.02 \
      -pseudo_plastic -pseudo_plastic_q 0.25 \
      -tauc_slippery_grounding_lines \
      -calving float_kill \
      -calving.float_kill.margin_only false \
      -calving.float_kill.calve_near_grounding_line false "

NN=24
firstnode=0
lastnode=24

RUNSTART=1778
RUNEND=1896

xmin=80793.
ymin=-2650282.
xmax=388422.
ymax=-2226046.

# Set paralell run options
PISM="taskset -c ${firstnode}-${lastnode} pismr -regional"

cmd="mpiexec -n $NN $PISM -i $BOOT \
    $PHYS \
    -regional.zero_gradient true \
    -stress_balance.sia.max_diffusivity 500000 \
```

https://doi.org/10.1017/aog.2026.10056 Published online by Cambridge University Press

```
    -extra_file ex_${OUTFILENAME}.nc -extra_times $RUNSTART:$EXDT:$RUNEND \
    -extra_vars $EXVARS \
    -ts_file ts_${OUTFILENAME}.nc -ts_times $RUNSTART:$TSTIME:$RUNEND \
    $CLIMATE -ys $RUNSTART -ye $RUNEND -o ${OUTFILENAME}.nc"
$PISM_DO $cmd
```

https://doi.org/10.1017/aog.2026.10056 Published online by Cambridge University Press